


Pockels effect in low-temperature rhombohedral BaTiO₃

Therese Paoletta¹ and Alexander A. Demkov^{1*}

Department of Physics, The University of Texas, Austin, Texas 78712, USA

 (Received 11 December 2020; accepted 22 December 2020; published 11 January 2021)

We report a first principles analysis of the linear electro-optic (EO) or Pockels effect in rhombohedral BaTiO₃ (BTO), the lowest temperature phase of this ferroelectric perovskite. Si-integrated BTO is a promising material for EO modulators in Si photonics, with applications in optical quantum computing. This requires a fundamental understanding of the Pockels effect in BTO at low temperature. Through density functional perturbation theory, we explore the origins of a strong Pockels response by examination of the components that make up the ionic contribution to the EO tensor. We identify the phonon modes dominating the EO response and establish their relation to the electronic structure and optical properties of the material.

DOI: [10.1103/PhysRevB.103.014303](https://doi.org/10.1103/PhysRevB.103.014303)

I. INTRODUCTION

The Pockels, or linear electro-optic (EO), effect describes the change in the refractive index of a crystal when an electric field is applied [1]. The effect would be particularly useful in silicon photonics, where it could bridge upcoming optical technology with conventional silicon devices. Unfortunately, silicon is not EO active due to its centrosymmetric nature. Strained silicon and other materials have been implemented in EO modulators in silicon photonics, boasting a competitive speed, broad bandwidth, and low power consumption [2–6]. Recently, barium titanate has been successfully integrated onto silicon photonic platforms to fabricate EO modulators based on the Pockels effect [7] that showed tremendous promise. The range of emergent applications of this technology includes intrachip data transmission [8], neuromorphic logic optical chips [9], and photonic integrated circuits for computing [10–12]. So far, research in this area has focused on room temperature applications. However, cryogenic conditions are required in certain types of quantum computing, radio astronomy, particle physics, and terahertz sensing [13]. Rhombohedral BaTiO₃, or rh-BTO (space group *R3m*), is the lowest temperature stable phase of barium titanate [14]. It is stable below 90 °C and is ferroelectric. Unfortunately, relatively little is known about the physical properties of this phase of BaTiO₃ [9,13].

Traditionally, the most common use of the Pockels effect is in the telecommunications industry, where lithium niobate LiNbO₃ (LNO) is used in optical modulators [15]. The effective Pockels coefficient of ~ 30 pm/V for LNO sets a “gold standard” for an appreciable Pockels response [16]. Additionally, LNO’s broad spectral range also makes it more attractive than other EO materials [17]. Some materials exhibit stronger responses, yet they are thermally and chemically unstable in the conditions needed for integration with silicon photonics [18]. BaTiO₃, however, has a much stronger Pockels response

(~ 1300 pm/V [19]), is chemically and thermally stable, can be integrated on silicon (001), and its use has already been demonstrated in a variety of applications, including silicon photonics [20–22]. The low-temperature response has only been recently reported and is very much diminished compared with the room temperature, tetragonal phase [13]. It is unclear whether this reduction comes from fundamental shifts in the material properties or from external factors such as strain, composition, or microstructure.

Here, we report a theoretical study of the EO response in rh-BTO. Using first principles calculations, we delve into the building blocks of the ionic contribution to the Pockels tensor. Specifically, we explore the Raman susceptibility, which “measures” how phonons couple to electrons, altering the electronic structure. The connection between the Raman susceptibility and electron-phonon coupling was first pointed out by Kaminow and Johnston [23] and recently discussed by Hamze *et al.* [24]. In this paper, we investigate why certain phonon modes exhibit larger Raman susceptibilities and dominate the Pockels response for rh-BTO. We analyze which intrinsic bonding properties strongly contribute to the response and consider how these could be enhanced via materials engineering.

II. BACKGROUND AND METHODS

The Pockels effect describes how the refractive index of a crystal changes under the influence of an applied electric field. It is traditional to introduce it in the context of a change in the optical indicatrix as follows [25]:

$$\Delta\left(\frac{1}{n_{ij}^2}\right) = \Delta(\varepsilon^{-1})_{ij} = \sum_{\gamma} r_{ij\gamma} E_{\gamma}. \quad (1)$$

But it can also be written as the first-order change to the dielectric tensor induced by an applied electric field E_{γ} [26]:

$$d\epsilon_{ij} = -\sum_k r_{ij\gamma} \epsilon_{ik} \epsilon_{kj} dE_{\gamma}(\omega). \quad (2)$$

*demkov@physics.utexas.edu

In piezoelectric crystals such as BaTiO₃, we expand the full differential of the dielectric tensor into purely electronic, lattice, and piezoelectric contributions [27]:

$$\begin{aligned} & \left[\frac{d\varepsilon_{ij}(R, \eta_0, E)}{dE_\gamma} \right]_{R_0, \eta_0, E=0} \\ &= \left[\frac{\partial \varepsilon_{ij}(R_0, \eta_0, E)}{\partial E_\gamma} \right]_{E=0} + 4\pi \sum_{\mu, \nu=1}^3 \left[\frac{\partial \chi_{ij}^{(1)}(R_0, \eta)}{\partial \eta_{\mu\nu}} \right]_{\eta_0} \eta_{\mu\nu}^{E_\gamma} \\ &+ 4\pi \sum_{k, \alpha} \left[\frac{\partial \chi_{ij}^{(1)}(R, \eta_0)}{\partial \tau_{k\alpha}} \right]_{R_0} \tau_{k\alpha}^{E_\gamma}. \end{aligned} \quad (3)$$

Here, E_γ is the electric field component in direction γ , R describes the ionic coordinates, $\eta_{\mu\nu}$ is the (μ, ν) element of the strain tensor describing the distortion due to the electric field, the naught refers to values at equilibrium, $\chi_{ij}^{(1)}$ is the linear dielectric susceptibility, and $\tau_{k\alpha}$ refers to displacement of atom κ in the α direction. The superscript E_γ denotes a derivative being taken with respect to the electric field.

The first term on the right-hand side of Eq. (3) represents the purely electronic contribution coming from the interaction of the electric field with valence electrons, assuming the ions are clamped at their equilibrium positions. It is related to the second harmonic generation effect. The electronic contribution can be written in terms of $\chi^{(2)}$, which is a third derivative of the electric enthalpy with respect to the electric field. In perovskites, this term tends to be relatively small [24].

The second term from the right represents the converse piezoelectric effect. If the frequency of the applied electric field is sufficiently high, this response will be ‘‘clamped,’’ referring to the lattice vectors staying constant. We assume the applied field frequency is low enough to trigger the converse piezoelectric effect and compute the full *unclamped* response. The unclamped Pockels tensor can be written in terms of the clamped Pockels tensor $r_{ij\gamma}^\eta$, the piezoelectric strain coefficients $d_{\gamma\mu\nu}$, and elasto-optic coefficients $p_{ij\mu\nu}$:

$$r_{ij\gamma}^\sigma = r_{ij\gamma}^\eta + \sum_{\mu, \nu=1}^3 p_{ij\mu\nu} d_{\gamma\mu\nu}. \quad (4)$$

The elasto-optic coefficients can be calculated directly using first principles software packages such as ABINIT (see below). However, the piezoelectric strain coefficients must be calculated separately. They are defined as the derivative of the inverse dielectric tensor with respect to strain. We rewrite Eq. (4) in terms of the inverse dielectric tensor and convert the derivative into a finite-difference form:

$$\Delta(\epsilon^{-1})_{ij}^{\text{piezo}} = \sum_{\mu, \nu=1}^3 p_{ij\mu\nu} \eta_{\mu\nu}, \quad (5)$$

$$p_{ij\mu\nu} \approx \frac{\Delta(\epsilon^{-1})_{ij}(\eta^+) - \Delta(\epsilon^{-1})_{ij}(\eta^-)}{2\eta_{\mu\nu}} + \mathcal{O}(\eta^2). \quad (6)$$

The η^\pm indicates that strain is applied to the unit cell when the dielectric tensor is calculated. Although strain involves a three-dimensional distortion of lattice vectors, here, it is formulated as a simple scalar. Thus, we evaluate the dielectric

tensor for different distortions of the unit cell using a centered, finite-difference derivative.

The last term in Eq. (3) represents the ionic contribution, resulting from the change in the dielectric tensor induced by changes in the atomic positions in response to the applied electric field. Given the minimum condition on electric enthalpy at the equilibrium positions, one can relate the second derivative with respect to $\tau_{k\alpha}$ (the force constant matrix in harmonic theory) to the first derivative of polarization with respect to $\tau_{k\alpha}$ (the Born effective charge $Z_{k\gamma\beta}^*$) [27]. We largely follow Veithen *et al.* [27], and the reader may see the Supplemental Material [28] with the full details of the derivation. Since the eigenvectors of the dynamical matrix form a complete set, $\tau_{k\alpha}^{E_\gamma}$ can be expressed in terms of the zone-center normal modes or the mass-normalized eigendisplacements, $u_m(k\alpha)$ [29]. Consequently, the second term can be written as:

$$4\pi \sum_m \frac{1}{\omega_m^2} \left[\sum_{k\alpha} \frac{\partial \chi_{ij}^{(1)}(R)}{\partial \tau_{k\alpha}} u_m(k\alpha) \right] \left[\sum_{k'\beta} Z_{k'\gamma\beta}^* u_m(k'\beta) \right]. \quad (7)$$

The derivative in the first bracket is the so-called Raman susceptibility, describing the modulation of the optical properties [linear dielectric susceptibility $\chi^{(1)}$] by lattice vibrations [23]. This is the very same mechanism that is responsible for Raman scattering. The second bracket is the mode polarity, which is comprised of the Born effective charge and the eigendisplacements. The zone center phonon frequencies are ω_m .

Clearly, the electronic susceptibility and its derivative are critical to the Pockels response. To gain some physical insight, consider a one-dimensional chain within a tight-binding (TB) theory, treating the electric field as a perturbation. In the limit of vanishing frequency, one can write [30]

$$\chi_{ij}^{(1)} = \frac{2\hbar^4 e^2}{m_e^2 \Omega_o} \sum_{n, n'} \frac{|\langle \psi_{n'} | \partial / \partial x | \psi_n \rangle|^2}{(\varepsilon_{n'} - \varepsilon_n)^3}. \quad (8)$$

The transition energy in the denominator is cubed, meaning that transitions between states with the smallest energy difference, such as those near the band edge, contribute the most. When a crystal vibrates, the displacement of the ions alters the band structure, with some modes affecting the electronic structure more than others. Consequently, we analyze how certain modes change the band gap, controlling the dominant term in the electronic susceptibility. As we will go on to show, the Pockels response depends on the derivative of the electronic susceptibility with respect to ionic displacement. We find that modes that stretch the bonds between titanium and oxygen are the ones that contribute strongly to the Pockels response.

As we have mentioned, the lowest temperature phase that has been observed for barium titanate is rhombohedral, with space group $R3m$, which is shown in Fig. 1. Through a series of phase transitions with increasing temperature, the crystal transforms from the ferroelectric rhombohedral to the ferroelectric orthorhombic ($T_c = -90^\circ\text{C}$), then to the ferroelectric tetragonal phase ($T_c = 5^\circ\text{C}$), and finally to the paraelectric cubic phase ($T_c = 120^\circ\text{C}$) [31].

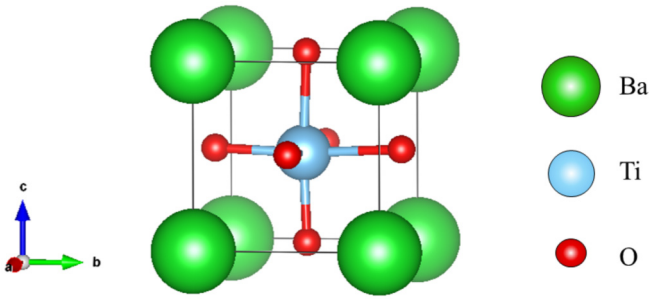


FIG. 1. Ball-and-stick model of rh-BaTiO₃. The distortion from the cubic cell is very slight (characteristic angle of 89.84°), and the titanium off-center displacement is along the body diagonal.

In the rhombohedral phase, all lattice vectors have equal length of 4.0036 Å, and the angle between them is 89.84° [14]. The atomic positions approximately follow the usual ABO₃ perovskite structure, with barium at the corners, and then both the oxygen and titanium are slightly displaced from the face centers and cell center, respectively. The Wyckoff positions for both the rhombohedral and hexagonal unit cell descriptions are given in Table I. These distortions give the phase its spontaneous polarization, with an experimental value of 33.5 μC cm⁻¹ [32]. The titanium is displaced along the body diagonal from the center by 0.0077 Å. The oxygens are all slightly displaced in the opposite direction along the body diagonal by about 0.043 Å.

All our calculations are performed within the framework of density functional theory (DFT), using the ABINIT [27,33–38] and VASP [39,40] software packages. In ABINIT, the local density approximation (LDA) [41,42] was used to calculate the exchange-correlation energy. We use Teter “extended” norm-conserving pseudopotentials with the valence electron configurations 5s²5p⁶6s² for the barium atom (*s* and *p* electrons included as semicore states), 3s²3p⁶4s²3d² for the titanium atom, and 2s²2p⁴ for the oxygen atoms [43]. We obtain a convergence of 2 × 10⁻⁵ Hartree = 5 × 10⁻⁴ eV/atom by using a plane-wave cutoff energy of 105 Hartree = 2850 eV and a 10 × 10 × 10 Monkhorst-Pack *k*-point grid [44] for all ABINIT calculations. We chose to work with a theoretically optimized lattice constant of 3.94 Å. Considering that LDA tends to underestimate lattice constants, this agrees well with the experimental value of 4.0036 Å [14]. The LDA band gap is probably underestimated. Hybrid exchange-correlation functionals, such as B3PW and B3LYP, tend to predict better band gaps for ABO₃ perovskites [45,46], but here, we use a simpler scissor correction when calculating the high-frequency dielectric tensor (discussed later). We work with the same lattice vectors in VASP. We use the same LDA functional

TABLE I. Wyckoff Positions for R3m BaTiO₃.

Site	Element	Rhombohedral		Hexagonal	
		Wyckoff	Symbol	Wyckoff	Symbol
Ba	Ba	1a	3m	9b	.m
Ti	Ti	1a	3m	3a	3m
O	O	3b	.m	3a	3m

TABLE II. Clamped and unclamped Pockels tensor r_{ij} for rhombohedral BaTiO₃.

Clamped EO tensor (pm/V)			Unclamped EO tensor (pm/V)		
0	26	55	0 ^a	69 ^a	63 ^a
0	-26	55	0 ^a	-69	63 ^a
0	0	113	0 ^a	0	123
0	81	0	0	206	0
81	0	0	206	0	0
26	0	0 ^a	69 ^a	0 ^a	0

^aWe transform to the principal axes after the density functional theory calculation runs to recover the correct symmetry, and imperfect values can lead to noise of about ~1 pm/V in the transformation.

[41] and projector augmented wave potentials that treat semicore *s* states as valence states in barium and titanium [40]. By using a plane-wave cutoff energy of 650 eV and a 16 × 16 × 16 Monkhorst-Pack *k*-point grid, we obtain a convergence of 5 × 10⁻⁵ eV/atom.

III. RESULTS AND DISCUSSION

Before discussing our results for the Pockels tensor, which has received little experimental attention in the rhombohedral phase, we compare another property, the dielectric tensor, to assess the validity of the calculations. Previously reported values of the high-frequency dielectric constant $\epsilon_{xx} = \epsilon_{yy} = 6.16$ and $\epsilon_{zz} = 5.69$ [47] are in good agreement with our values of $\epsilon_{xx} = \epsilon_{yy} = 6.56$ and $\epsilon_{zz} = 6.48$. We also compare with the experimental value based on an average refractive index of 2.28 [13], giving $\epsilon_{ii} = 5.20$. When we use a scissor correction for the band gap, we obtain $\epsilon_{xx} = \epsilon_{yy} = 5.57$ and $\epsilon_{zz} = 5.51$, in good agreement with experiment.

The Pockels tensor has three indices, the first two referring to the directions of the propagating light (the indicatrix) and the third to the direction of the applied electric field. The tensor is symmetric in the first two indices, so it may be collapsed using Voigt notation. We report both the clamped and unclamped EO tensors in Table II. The largest component of the clamped tensor is $r_{33} = 113$ pm/V, while for the unclamped it is $r_{51} = r_{42} = 206$ pm/V. These are both much larger than $r_{33} = 33.5$ pm/V for unclamped lithium niobate [48], but significantly less than those of the tetragonal phase of BTO [49]. Also, the piezoresponse contributes almost half of the total, suggesting a large difference for the effect measured at high and low frequency.

Recently, the clamped effective Pockels coefficient of a thin BaTiO₃ film was reported to be 200 pm/V at 4 K [13]. Although BaTiO₃ would usually assume the rhombohedral phase at 4 K, we hesitate to say the observed phase is necessarily rh-BTO. The sample in that study was a thin film grown on SrTiO₃-buffered silicon by molecular beam epitaxy, a process that often leads to strain caused by thermal and lattice mismatch [21,50]. Strain alters the temperature when a phase transition would usually occur in thin films [51], so the authors attempt to identify the phase, which cannot be inferred from temperature alone. They argue that certain signatures, such as abrupt changes in the EO value, indicate a phase transition to the rhombohedral phase. Considering the

TABLE III. Phonon frequencies at the Γ point, divided into transverse and longitudinal modes. All the transverse modes are doubly degenerate.

Mode type	SR freq. (cm ⁻¹)	LR freq. (cm ⁻¹)	Theory freq. (cm ⁻¹) [53]	Exptl. freq. (cm ⁻¹) [54]
TO	91	91	145	–
	187	187	191	173
	292	292	306	242
	491	491	489	522
LO	120	184	193	187
	184	288	297	Silent
	288	463	471	485
	501	702	713	714

thermal properties of phonons, however, could also explain the abrupt change in the EO response. As the temperature drops, fewer phonon modes can be excited. Let us assume that all key modes contribute at the rhombohedral-orthorhombic phase transition temperature of 183 K and ignore the slight temperature dependence of frequencies. Then for simplicity, upon cooling, once a mode's Bose-Einstein occupation number drops to $1/e$ of its value at the phase transition, let's exclude that mode's contribution. Our calculations indicate that the r_{13} , r_{23} , and r_{33} elements will vanish at 103 K. Then at 96 K, the entire ionic response freezes out, which would reduce the total Pockels response by about 50% of its original value, as only the electronic and piezoelectric responses remain. Overall, our calculations suggest that having such a large, clamped response at 4 K suggests that a phase other than rhombohedral might be present in the thin film. On the other hand, given the number of effects that can alter the EO response (such as strain and composition), the reported value agrees fairly with our maximum clamped component of 113 pm/V.

We compare our calculated phonon frequencies with other theoretically and experimentally obtained values in Table III and find good agreement. For clarity, in the next section, we report both the long-range (LR), corrected and uncorrected, short-range vibrational frequencies. In ionic crystals, longitudinal modes are affected by the LR Coulomb force, as captured by the Lydanne-Sachs-Teller (LST) relation [52]. The LR-corrected values are relevant for comparison with Raman spectroscopy [54]. Only the transverse modes that do not require the LST correction enter the Pockels calculation; we will mention these frequencies in a later part. Note that all the transverse modes are doubly degenerate.

To gain further insight into the origins of the large value of the EO coefficient, let us consider the three elements that constitute the ionic EO response: The Raman susceptibility, the mode polarity, and the Γ point frequencies. We express the ionic contribution of Eq. (7) more compactly by introducing α_{ij}^m , the Raman susceptibility, and $p_{m,\gamma}$, the mode polarity:

$$r_{ij\gamma}^{\text{ion}} = -\frac{4\pi}{\sqrt{\Omega_0} n_i^2 n_j^2} \sum_m \frac{\alpha_{ij}^m p_{m,\gamma}}{\omega_m^2}. \quad (9)$$

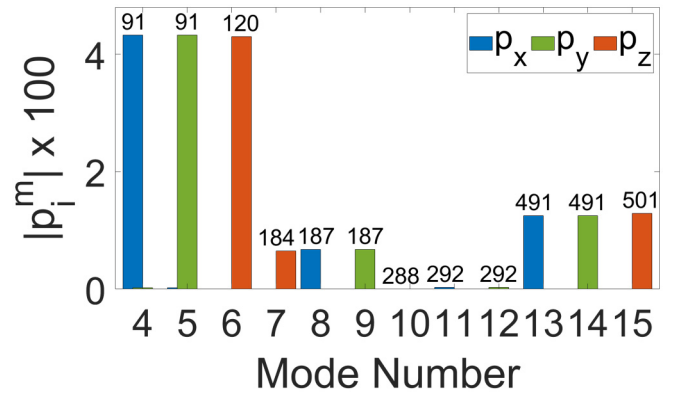


FIG. 2. Mode polarities of the Γ point lowest frequency optical modes of rh-BTO. The number above each column indicates the mode frequency in cm⁻¹. The units of the mode polarity are $e \times \text{Bohr}$, where e is the electron charge.

The mode polarity, which measures the dipole moment a phonon creates, is defined as follows:

$$p_{m,\gamma} = \sum_{\kappa,\beta} Z_{\kappa,\gamma\beta}^* u_m(\kappa\beta). \quad (10)$$

The eigendisplacements $u_m(\kappa\beta)$ are bound by normalization conditions and temperature. Thus, the mode polarity is not likely to produce a very large EO response, but it can diminish it. The mode polarity for each mode has a component for each Cartesian direction. We plot the three elements for the 12 lowest frequency optical modes in Fig. 2.

The lowest frequency modes 4–6 have the largest polarities, each having one nonzero component along the three Cartesian coordinates. Each set of three modes similarly has one nonzero component of equal magnitude, but with lower strength compared with modes 4–6. By definition, the Born effective charge is mode independent. In modes 4–6 (the corresponding displacements are illustrated in Fig. 3), the distance between the anions and cations varies strongly, enhancing the dipole moment compared with other modes.

Figure 4 shows the displacement patterns for every mode by plotting the magnitude (absolute value) of every atom's eigendisplacement. Modes 4–6 are unique in that they feature the titanium moving with equal magnitude but in the opposite direction as the oxygen, and the barium is frozen out. In general, barium barely moves, except in modes 7–9. In these modes, the titanium and oxygen move together along one direction, while the barium moves in the opposite direction. This behavior differs from tetragonal BTO, where the barium generally does not move at all. In modes 10–12 and 13–15, the movements are limited to oxygen with no clear relational patterns.

Next, we analyze the Raman susceptibility, which can be obtained by expanding the derivative of the dielectric tensor that is directly related to the susceptibility in terms of ionic displacements:

$$\alpha_{ij}^m = \sqrt{\Omega_0} \sum_{\kappa,\beta} \frac{\partial \chi_{ij}^{(1)}}{\partial \tau_{\kappa\beta}} u_m(\kappa\beta). \quad (11)$$

We plot the largest component of the Raman tensor for the 12 lowest frequency optical modes in Fig. 5.

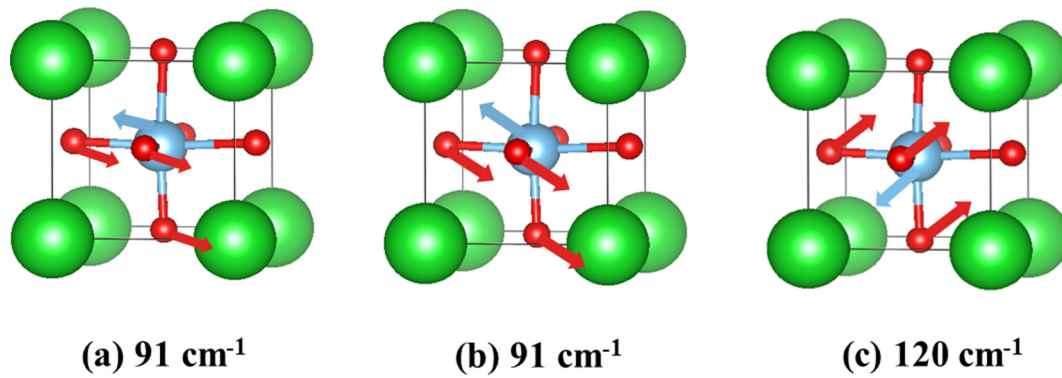


FIG. 3. Displacement patterns for modes 4–6 that dominate the Pockels response. All feature oxygens and titanium moving in the opposite directions, thus stretching the bond length. (a) Mode 4: The oxygens move like a rigid octahedron in the $[0\bar{1}\bar{1}]$ direction. (b) Mode 5: The oxygens move nearly uniformly in the $[2\bar{1}\bar{1}]$ direction, while titanium moves in the opposite direction. (c) Mode 6: The three oxygens move nearly uniformly in the $[111]$ directions, while titanium moves in the opposite direction.

Like the mode polarities, the Raman susceptibilities of the first three optical modes are the largest. To emphasize how the pairing of a large Raman susceptibility with low frequencies gives an especially large Pockels response, the modes are labeled by their respective frequencies. Since the mode frequencies enter the ionic contribution as a squared factor in the denominator, the combination of small frequencies with large polarities and Raman susceptibilities leads to a large Pockels response.

As Eq. (11) suggests, the critical element of the Raman susceptibility is the derivative of the linear dielectric susceptibility with respect to atomic displacement, $\frac{\partial \chi_{ij}}{\partial \tau_{\kappa\alpha}}$. Of the 135 elements of this derivative, six have amplitudes that are orders of magnitude larger than the rest. These six elements correspond to titanium and oxygen moving along the Ti-O bond along the three Cartesian directions. We find that modes that stretch this bond play a large role in the Pockels response, making them “active” modes (see below).

Consider, for example, how modes 6 and 10 impact the electronic structure. Equation (8) suggests that the smallest

energy transitions control the magnitude of the susceptibility. The band gap transition would be the leading term in this sum, so we investigate the dependence of the gap on the displacements of these two modes. In Fig. 6, we plot the change in the band gap when the ions take on positions determined by the eigendisplacements for increasing magnitudes of displacements. We define the amplitude as the absolute value of the largest component of the displacement pattern (also known as the supremum norm). To choose the modes to analyze, we did the following: using Eq. (11), each mode m has a 3×3 Raman susceptibility matrix with subscripts ij . For every mode, we took the element of the Raman susceptibility tensor with the greatest magnitude. Then we chose the greatest and least elements of the 12 optical modes, which correspond to modes 6 and 10, respectively, which we call the Raman active and inactive modes. These also happen to be the modes that contribute the most and the least to the Pockels tensor.

The plot shows that the Raman inactive mode hardly changes the band gap, while the active mode considerably does. Equation (8) shows that the strong dependence of the band gap on ionic displacements results in a larger $\frac{\partial \chi}{\partial \tau}$, ensuring a large ionic EO response. In this example, the positive displacement (bond stretch) results in the gap closing.

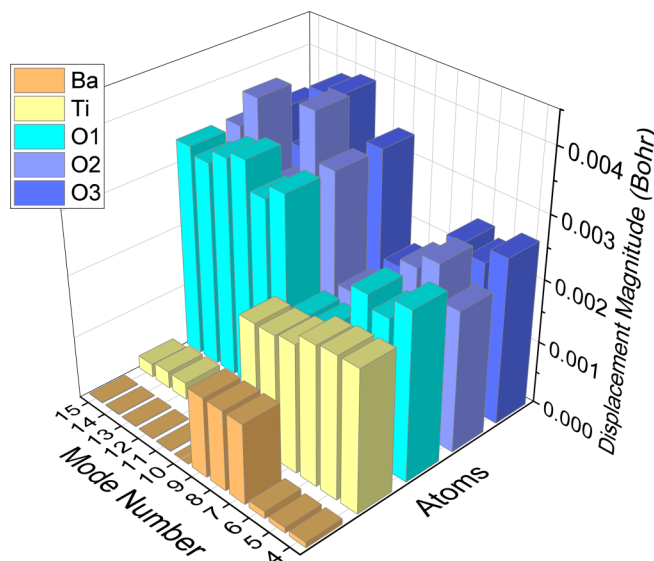


FIG. 4. Magnitudes of displacement of each atom for all optical modes at the Γ point.

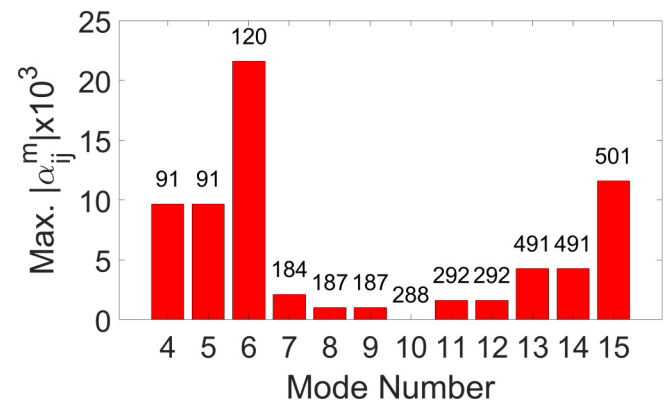


FIG. 5. Raman susceptibility for the Γ point optical modes, labeled by the mode number with the unboosted (see text) frequencies shown above each bar. The units of the Raman susceptibility are Bohr $^{3/2}$, coming from the square root of the unit cell volume.

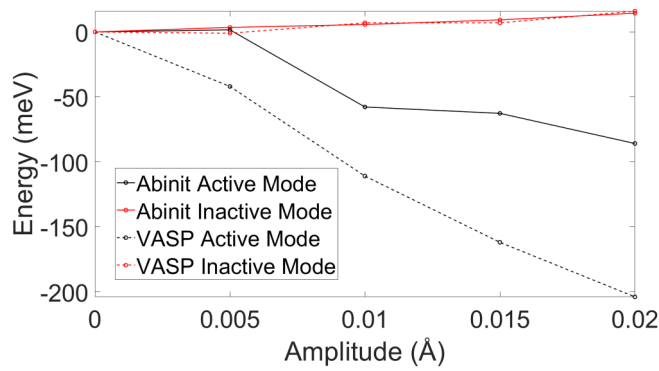


FIG. 6. The change in the band gap for different magnitudes of displacement. We calculated this dependence in both ABINIT and VASP.

We can relate this to the specific orbitals that control the band broadening near the conduction band minimum. This dependence highlights the connection between modes with large Raman (and thus Pockels) responses and electron-phonon coupling [23,24].

To better understand what drives the change in the band gap for these modes, we draw on molecular orbital theory. Oxygen has three types of p states, while titanium has five types of d states, the types referring to the magnetic quantum number. In the Hückel TB theory [55], the magnitude of the off-diagonal matrix elements is taken to be proportional to the orbital overlap. The overlap of each orbital's wave function with another is determined by the distance between the atoms and the alignment of the orbitals. Phonons displace ions and can therefore change the TB parameters. See Fig. 7 for a schematic of the orbital geometry.

There are two groups of bonding and antibonding states formed by the orbitals on oxygen and titanium. Using the crystal field theory terminology, these are called e_g and t_{2g} , with a star denoting the antibonding states. The bands near the conduction band minimum are made up of titanium-oxygen antibonding states (t_{2g}^* , made up of $d_{xy}, d_{yz},$ and d_{zx}), while the bands near the valence band maximum are the so-called nonbonded oxygen states [56]. As an example, we plot the density of states (DOS) near the band gap for our equilibrium

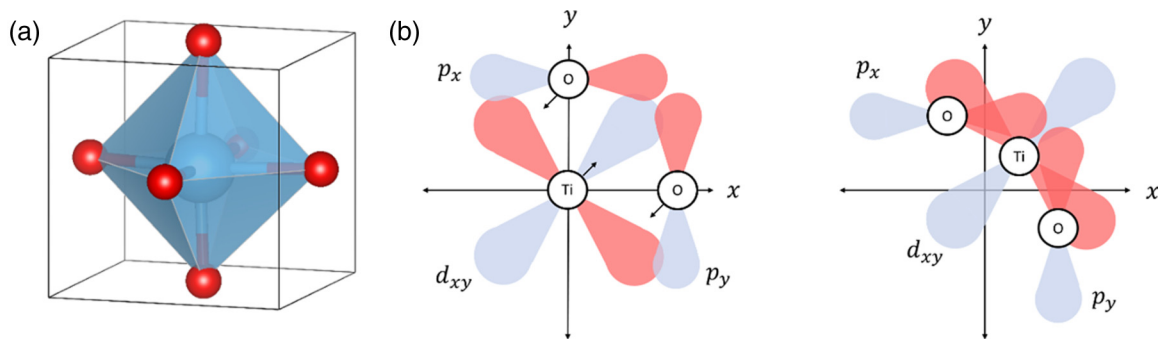


FIG. 7. (a) A three-dimensional picture of the TiO_6 octahedron. (b) A top view of the octahedron, with example orbitals placed on the ions. The three types of $2p$ orbitals were assigned to each oxygen with no particular meaning, and the titanium $3d_{xy}$ was chosen as an example t_{2g}^* state. The lobe coloring refers to the sign of the phase of the wave function, red being positive and blue negative. The picture on the left shows the orbitals before a phonon displacement, with arrows indicating how the ions and their orbitals will move. The picture on the right shows how the orbitals would overlap with phonon displacement. One can see that the angle between bonds and the bond length strongly affect how these orbitals overlap.

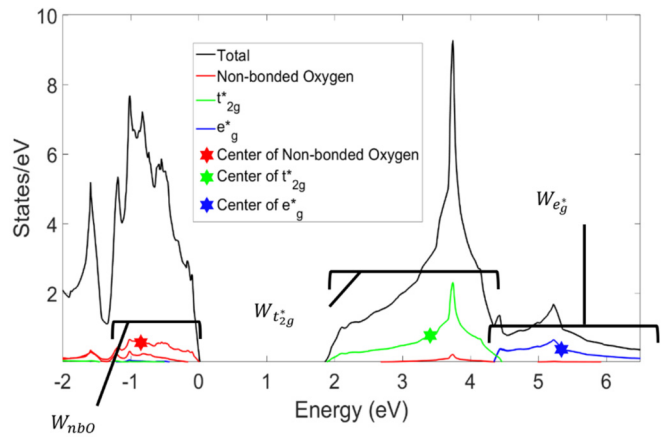


FIG. 8. Density of states (DOS) for rh-BTO (a cell with lattice constant of 3.94 \AA is used). The plot includes the total DOS and the orbital-projected contributions for each atom. The width of the bands is denoted by the black bars with the orbital named attached. The center is marked by a star with the color corresponding to the legend.

volume crystal, with both the total and partial densities of states (PDOS) in Fig. 8.

Phonons alter the instantaneous ionic positions and thus the bonding properties of the crystal. We studied how the active and inactive modes mentioned above affect the width and “center of gravity” of the bands controlling the band gap. In the Supplemental Material [28], we plot the various characteristics as a function of displacement amplitude. The two main mechanisms behind the change of the band gap as the active phonon amplitude grows is the t_{2g}^* band widening and the nonbonded oxygen center of gravity shifting upward. The former points to hopping between the O $2p$ and Ti $3d$ states becoming easier or the hopping integral increasing. The hopping matrix element can be approximated as an empirical parameter times the overlap integral, which suggests that the overlap integrals between the O $2p$ and Ti $3d$ states change, causing the Pockels response to increase.

This relationship can be understood by considering the ionic displacements of the titanium and oxygen. In the equi-

TABLE IV. Clamped Pockels tensor for several lattice constants of rhombohedral BaTiO₃ (in pm/V).

Latt. constant 3.93 Å	Latt. constant 3.94 Å	Latt. constant 3.97 Å	Latt. constant 4.00 Å
$\begin{bmatrix} 0 & 36 & 90 \\ 0 & -36 & 90 \\ 0 & 0 & 174 \\ 0 & 111 & 0 \\ 111 & 0 & 0 \\ 36 & 0 & 0 \end{bmatrix}$	$\begin{bmatrix} 0 & 22 & 47 \\ 0 & -22 & 47 \\ 0 & 0 & 88 \\ 0 & 69 & 0 \\ 69 & 0 & 0 \\ 22 & 0 & 0 \end{bmatrix}$	$\begin{bmatrix} 0 & 10 & 24 \\ 0 & -10 & 24 \\ 0 & 0 & 45 \\ 0 & 36 & 0 \\ 36 & 0 & 0 \\ 10 & 0 & 0 \end{bmatrix}$	$\begin{bmatrix} 0^a & -6 & 16 \\ 0^a & 6 & 16 \\ 0^a & 0 & 31 \\ 0 & 24 & 0 \\ 24 & 0 & 0 \\ -6 & 0 & 0 \end{bmatrix}$

^aWe transform to the principal axes after the DFT calculation runs to recover the correct symmetry, and imperfect values can lead to noise of about ~ 1 pm/V in the transformation.

librium structure, the O-Ti-O bonds form a three-dimensional chain, where every unit cell has two different Ti-O bond lengths, due to the ferroelectric distortion. In the active mode, the three oxygens and titanium in the unit cell move in the exact opposite directions, which means they are moving closer to another cell for three other pairs. This motion leads to the maximum change in the overlap integral for the t_{2g}^* states. We quantify this by looking at the change in the bond length and the O-Ti-O bond angle. Using the active mode displacement with maximum amplitude, the sum of the change in the bond length of the six Ti-O bonds is 9.13%. This change reduces the difference between each pair of bond lengths that form a chain, making the rhombohedral octahedron more like the cubic one. Comparatively, in the inactive mode, the difference in sum of bond lengths is only 0.06%. We also examine how the O-Ti-O bond angle changes. For the active mode, all the bond angles slightly increase from 175.6° to 177.8° , while the inactive results in a paltry 0.23° change. This motion also makes the unit cell resemble the cubic one more. Once again, we see the inactive mode hardly changes the unit cell in ways that control the bonding properties.

We note that all calculations were completed with a lattice constant that was theoretically optimized. However, LDA tends to underestimate lattice constants, and the rhombohedral phase exists at finite temperatures, which leads to thermal expansion. Thus, there is some uncertainty in what lattice constant to use to predict experimental values. Consequently, we calculated the EO response for several volumes, and the results are listed in Table IV. For each lattice constant, we allowed the ions to relax while maintaining the same characteristic angle and space group of the unit cell. Note we did not apply scissor corrections to the band gap for these values.

The results show that starting with the experimental volume, the Pockels response increases as the cell volume decreases. As the cell gets smaller, it maintains its space group, but the reduced coordinates begin to resemble those of the centrosymmetric cubic cell, reducing the shifts that give the cell its ferroelectric polarization. This centering of the atoms and decrease of interatomic distance increases the overlap of neighboring O $2p$ and Ti $3d$ orbitals. As the volume shrinks, the band gap closes, as the t_{2g}^* band widens.

Additionally, the frequencies of modes 4–6 decrease rather steeply as the cell gets smaller, driving up the ionic term. Mode softening often points to a phase transition, and previous papers have discussed the possibility of using strain to enhance BTO's response via softening the modes in the vicinity of a morphotropic boundary for the tetragonal phase [57]. As we decrease the cell volume, the lowest transverse mode of 17 cm^{-1} occurs for a lattice constant of 3.93 Å, and we find instabilities of up to $-8i \text{ cm}^{-1}$ near but not at Γ . The mode softening does clearly heighten the Pockels response for these other volumes, as the Raman susceptibilities in fact diminish. So although the rhombohedral phase does not have quite as large a response as other phases, with proper strain engineering, it could possibly be enhanced.

IV. CONCLUSIONS

We report the first principles study of the Pockels tensor for low-temperature rhombohedral BaTiO₃. The cryogenic conditions necessary for optical quantum computing and other applications make this an important phase for using EO modulators based on the Pockels effect in Si-integrated BTO films. We identify the modes having greater Raman susceptibilities and therefore large contribution to the EO response. We show how their displacement patterns induce changes in Ti-O bonding that strongly affect the band gap and electronic susceptibility. We have also discovered that these same modes are quite sensitive to strain. The significant increase in the Pockels response due to the softening of those modes points to the possibility of enhancing the EO response with strain engineering. Understanding the origins of the Pockels response is critical for identifying new material candidates and improving the known ones. This paper on rh-BTO identifies a fundamental mechanism controlling the large response and suggests the possibility of using strain to enhance the response.

ACKNOWLEDGMENT

We thank Agham Posadas and Marc Reynaud for insightful discussions. This paper is supported by the Air Force Office of Scientific Research under Grant No. FA9550-18-1-0053.

- [1] J. F. Nye, *Physical Properties of Crystals* (Clarendon Press, Oxford, 1985).
 [2] G. T. Reed, G. Mashanovich, F. Y. Gardes, and D. J. Thomson, *Nat. Photon.* **4**, 518 (2010).

- [3] M. J. R. Heck, H.-W. Chen, A. W. Fang, B. R. Koch, D. Liang, H. Park, M. N. Sysak, and J. E. Bowers, *IEEE J. Sel. Top. Quantum Electron.* **17**, 333 (2011).

- [4] J. Gourlay, M. Forbes, and M. Desmulliez, *Electron. Commun. Eng. J.* **13**, 221 (2001).
- [5] A. F. Benner, M. Ignatowski, J. A. Kash, D. M. Kuchta, and M. B. Ritter, *IBM J. Res. Dev.* **49**, 755 (2005).
- [6] M. Li and H. X. Tang, *Nat. Mater.* **18**, 9 (2019).
- [7] F. Eltes, C. Mai, D. Caimi, Y. Popoff, G. Winzer, D. Petousi, S. Lischke, J. E. Ortmann, L. Czornomaz, L. Zimmermann, J. Fompeyrine, and S. Abel, *J. Lightwave Tech.* **37**, 1456 (2019).
- [8] K. Yamada, Y. Urino, T. Nakamura, and Y. Arakawa, *NTT Tech. Rev.* **11**, 1 (2013).
- [9] S. Abel, F. Eltes, J. E. Ortmann, A. Messner, P. Castera, T. Wagner, D. Urbonas, A. Rosa, A. M. Gutierrez, D. Tulli, P. Ma, B. Baeuerle, A. Josten, W. Heni, D. Caimi, L. Czornomaz, A. A. Demkov, J. Leuthold, P. Sanchis, and J. Fompeyrine, *Nat. Mater.* **18**, 42 (2019).
- [10] T. D. Ladd, F. Jelezko, R. Laflamme, Y. Nakamura, C. Monroe, and J. L. O'Brien, *Nature* **464**, 45 (2010).
- [11] J. L. O'Brien, A. Furusawa, and J. Vučković, *Nat. Photon.* **3**, 687 (2009).
- [12] J. Wang, F. Sciarrino, A. Laing, and M. G. Thompson, *Nat. Photon.* **14**, 273 (2019).
- [13] F. Eltes, G. E. Villarreal-Garica, D. Caimi, H. Siegart, A. A. Gentile, A. Hart, P. Stark, G. D. Marshall, M. G. Thompson, J. Barreto, J. Fompeyrine, and S. Abel, *Nat. Mater.* **19**, 1164 (2020).
- [14] G. H. Kwei, A. C. Lawson, S. L. Billinge, and S. W. Cheong, *J. Phys. Chem.* **97**, 2368 (1993).
- [15] E. L. Wooten, K. M. Kiss, A. Yi-Yan, E. J. Murphy, D. A. Lafaw, P. F. Hallemeier, D. Maack, D. V. Attanasio, D. J. Fritz, G. J. McBrien, and D. E. Bossi, *IEEE J. Sel. Top. Quantum Electron.* **6**, 69 (2000).
- [16] D. Janner, D. Tulli, M. Garcia-Granda, M. Belmonte, and V. Pruneri, *Laser Photon. Rev.* **3**, 301 (2009).
- [17] M. Leidinger, S. Fieberg, N. Waasem, F. Kühnemann, K. Buse, and I. Breunig, *Opt. Exp.* **23**, 21690 (2015).
- [18] F. Eltes, M. Kroh, D. Caimi, C. Mai, Y. Popoff, G. Winzer, D. Petousi, S. Lischke, J. E. Ortmann, L. Czornomaz, L. Zimmermann, J. Fompeyrine, and S. Abel, in *Proceedings of the 2017 IEEE International Electron Devices Meeting (IEDM)* (IEEE, San Francisco, 2017), p. 24.5.1.
- [19] R. Boyd, *Nonlinear Optics*, 3rd ed. (Academic Press, San Diego, CA, 2008).
- [20] K. J. Kormondy, S. Abel, F. Fallegger, Y. Popoff, P. Ponath, A. B. Posadas, M. Sousa, D. Caimi, H. Siegart, E. Uccelli, L. Czornomaz, C. Marchiori, J. Fompeyrine, and A. A. Demkov, *Microelectron. Eng.* **147**, 215 (2015).
- [21] C. Dubourdieu, J. Bruley, T. M. Arruda, A. Posadas, J. Jordan-Sweet, M. M. Frank, E. Cartier, D. J. Frank, S. V. Kalinin, A. A. Demkov, and V. Narayanan, *Nat. Nanotechnol.* **8**, 748 (2013).
- [22] A. Rosa, D. Tulli, P. Castera, A. M. Gutierrez, A. Griol, M. Baquero, B. Vilquin, F. Eltes, S. Abel, J. Fompeyrine, and P. Sanchis, *Opt. Mater. Express* **7**, 4328 (2017).
- [23] I. P. Kaminow and W. D. Johnston, *Phys. Rev.* **160**, 3519 (1967).
- [24] A. K. Hamze, M. Reynaud, J. Geler-Kremer, and A. A. Demkov, *npj Comput. Mater.* **6**, 130 (2020).
- [25] I. P. Kaminow and E. H. Turner, *Appl. Opt.* **5**, 1612 (1966).
- [26] S. H. Wemple and M. DiDomenico, *Appl. Solid State Sci.* **3**, 263 (1972).
- [27] M. Veithen, X. Gonze, and P. Ghosez, *Phys. Rev. B* **71**, 125107 (2005).
- [28] See Supplemental Material at <http://link.aps.org/supplemental/10.1103/PhysRevB.103.014303> for details of the derivation discussed in the text.
- [29] A. K. Hamze and A. A. Demkov, *Phys. Rev. Materials* **2**, 115202 (2018).
- [30] W. A. Harrison, *Electronic Structure and the Properties of Solids: The Physics of the Chemical Bond* (Dover Publications, New York, 1989).
- [31] P. R. Potnis, N. Tsou, and J. Huber, *Materials* **4**, 417 (2011).
- [32] A. W. Hewat, *Ferroelectrics* **6**, 215 (1973).
- [33] X. Gonze, *Phys. Rev. B* **55**, 10337 (1997).
- [34] X. Gonze and C. Lee, *Phys. Rev. B* **55**, 10355 (1997).
- [35] X. Gonze, *Z. Kristallogr. Cryst. Mater.* **220**, 558 (2005).
- [36] X. Gonze *et al.*, *Comput. Phys. Commun.* **180**, 2582 (2009).
- [37] X. Gonze *et al.*, *Comput. Phys. Commun.* **248**, 107042 (2020).
- [38] D. R. Hamann, X. Wu, K. M. Rabe, and D. Vanderbilt, *Phys. Rev. B* **71**, 035117 (2005).
- [39] G. Kresse and J. Hafner, *Phys. Rev. B* **47**, 558 (1993); G. Kresse and J. Furthmüller, *Comput. Mater. Sci.* **6**, 15 (1996); *Phys. Rev. B* **54**, 11169 (1996); G. Kresse and J. Hafner, *J. Phys.: Condens. Matter* **6**, 8245 (1994); G. Kresse and D. Joubert, *Phys. Rev. B* **59**, 1758 (1999).
- [40] P. E. Blöchl, *Phys. Rev. B* **50**, 17953 (1994).
- [41] D. M. Ceperley and B. J. Alder, *Phys. Rev. Lett.* **45**, 566 (1980).
- [42] J. P. Perdew and A. Zunger, *Phys. Rev. B* **23**, 5048 (1981).
- [43] M. Teter, *Phys. Rev. B* **48**, 5031 (1993).
- [44] H. J. Monkhorst and J. D. Pack, *Phys. Rev. B* **13**, 5188 (1976).
- [45] R. I. Eglitis and A. I. Popov, *J. Saudi Chem. Soc.* **22**, 459 (2018).
- [46] R. I. Eglitis, J. Purans, J. Gabrusenoks, A. I. Popov, and R. Jia, *Crystals* **10**, 745 (2020).
- [47] P. Ghosez, X. Gonze, and J. P. Michenaud, *Europhys. Lett.* **33**, 713 (1996).
- [48] Y. Shuto and M. Amano, *J. Appl. Phys.* **77**, 4632 (1995).
- [49] M. Zgonik, B. Bernasconi, M. Duelli, R. Schlessler, P. Günter, M. H. Garret, D. Rytz, Y. Zhu, and X. Wu, *Phys. Rev. B* **50**, 5941 (1994).
- [50] J. Nordlander, F. Eltes, M. Reynaud, J. Nürnberg, G. De Luca, D. Caimi, A. A. Demkov, S. Abel, M. Fiebig, J. Fompeyrine, and M. Trassin, *Phys. Rev. Materials* **4**, 034406 (2020).
- [51] N. Setter, D. Damjanovic, L. Eng, G. Fox, S. Gevorgian, S. Hong, A. Kingon, H. Kohlstedt, N. Y. Park, G. B. Stephenson, I. Stolitchnov, A. K. Tagansteve, D. V. Taylor, T. Yamada, and S. Streiffner, *J. Appl. Phys.* **100**, 051606 (2006).
- [52] G. K. Horton and A. A. Maradudin, *Dynamical Properties of Solids* (North-Holland, Amsterdam, 1974).
- [53] R. A. Evarestov and A. V. Bandura, *J. Comp. Chem.* **33**, 1123 (2012).
- [54] D. A. Tenne, X. X. Xi, Y. L. Li, L. Q. Chen, A. Soukiasian, M. H. Zhu, A. R. James, J. Lettieri, D. G. Schlom, W. Tian, and X. Q. Pan, *Phys. Rev. B* **69**, 174101 (2004).
- [55] E. Hückel, *Z. Phys.* **70**, 204 (1931).
- [56] T. Wolfram and S. Ellialtıoglu, *Electronic and Optical Properties of d-Band Perovskites* (Cambridge University Press, Cambridge, 2009).
- [57] K. D. Fredrickson, V. V. Vogler-Neuling, K. J. Kormondy, D. Caimi, F. Eltes, M. Sousa, J. Fompeyrine, S. Abel, and A. A. Demkov, *Phys. Rev. B* **98**, 075136 (2018).